Journal of Materials Chemistry A

Accepted Manuscript

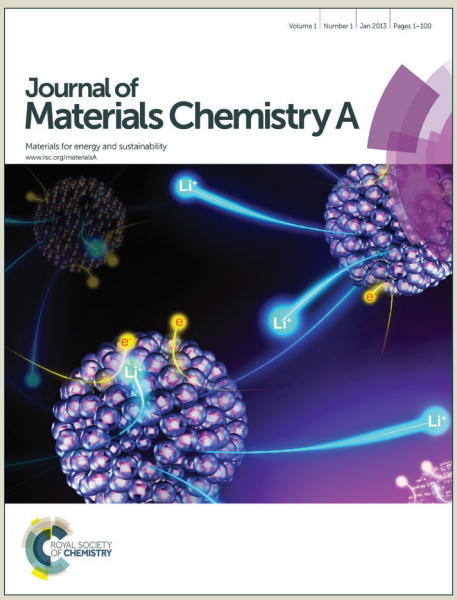

ROYAL SOCIETY OF CHEMISTRY

www.rsc.org/materialsA

Cite this: DOI: 10.1039/c0xx00000x

www.rsc.org/xxxxxx

ARTICLE TYPE

A new type of hybrid nanostructures: complete photo-generated carriers separation and ultrahigh photocatalytic activity

Yaguang Li[a,b], and Liping Zhu [a,b], Yanmin Guo[a,b], Hui Song[a,b], Zirui Lou[a,b], Zhizhen Ye[a,b]*

Received (in XXX, XXX) Xth XXXXXXXXX 20XX, Accepted Xth XXXXXXXXX 20XX

DOI: 10.1039/b000000x

In this work, we obtained a new type of hybrid nanostructures which are formed in an ultrathin shell of the mixed metal oxides hollow spheres. This new type of hybrid nanostructures exhibited a completely separation of the photo-generated hole-electron pairs and an ultrahigh photocatalytic activity which had never seen before. Using the TiO_2/SnO_2 hybrid nanostructure as an example, we found the presented hybrid nanostructures not only have the small grain size and ultrahigh surface area but also the important is the excellent crystalline compatibility and single-layer distributed arrangement for each nanoheterojunctions. Thus, this unique structure leads to the completely carrier's separation and the excellent photocatalytic activity. The typical method has been extended to synthesize other hybrid nanostructures successfully. We believe our methodology provides a general route to synthesis the new type of hybrid nanostructures for resulting applications.

Introduction

Semiconductor photocatalysis has been received much attention as a potential solution for energy shortages and environmental pollution.[1-3] However, the recombination of photo-generated electron and hole pairs is strikingly in the semiconductors[4, 5] and it is the significant and inherent drawback for most of the semiconductors.[6-8] Therefore, efficiently separate the photo-generated carriers is the state of the art for semiconductor photocatalysis.[9-11] To realize the efficient carriers' separation, semiconductor hybrid nanostructures, consisting of various semiconductors, have played an important role in modern photocatalysis.[12-15] In the previous work, a considerable number of hybrid nanostructures have been prepared by various preparation methods,[16-19] but efforts to enhance carriers transport are less. However, there are some inherent limitations in the hybrid nanostructures synthesized by conventional methods.[20-23] Firstly, the crystalline incompatibility between various materials are harmful to the separation of the photo-generated carriers.[20,24] Furthermore, the stacking nature of the existing hybrid nanostructures leads to the secondary recombination of the separated carriers at the inefficient interfaces between different nanoheterojunctions.[25,26] Therefore, it is of great interest to develop a new type of hybrid nanostructures to separate and transport the photo-generated carriers efficiently.

In this work, we designed a new type of hybrid nanostructures in the shell of hollow spheres by a facile ions adsorption and carbon templates approaches. Using the TiO_2/SnO_2 hybrid nanostructure as a typical example, we found this new type of hybrid nanostructures has excellent crystalline compatibility and monolayer distribution structure compared with the previous synthesized TiO_2/SnO_2 hybrid nanostructures.[13-17] This new hybrid nanostructure caused the carriers to be completely separated rather than the partly separation in conventional TiO_2/SnO_2 hybrid nanostructures.[13-17] Moreover, their surface areas are higher than 300 $m^2 g^{-1}$ which could facilitate the carriers transport to the surface. Therefore, this new type of hybrid nanostructures exhibited an ultrahigh photocatalytic efficiency. We further applied this strategy to fabricate other hybrid nanostructures successfully; therefore, it is an attractive way to fabricate the ideal hybrid nanostructures for resulting applications.

Experimental Section

Materials Synthesis

The carbon spheres were hydrothermally synthesized using the method reported by Li et al.[27] For the synthesis of this new type of hybrid nanostructures, we took the TiO_2/SnO_2 hybrid nanostructures as example, 0.5 g of carbon spheres were dispersed in 100 mL anhydrous ethanol by ultrasonication, followed by adding moderate amount of Tetrabutyl titanate and $SnCl_2 \cdot 2H_2O$. The obtained mixture was stirred for 24 h. A rinsing process involving two cycles of centrifugation/washing/re-dispersion was performed with ethanol. After dried in an oven at 80 °C for 6 h, the TiO_2/SnO_2 hollow spheres were obtained by calcinations the products in air at 350 °C for 12 h. And the hybrid nanostructures were obtained by annealing the hollow spheres in air at 450 °C for 12 h. The synthesis of TiO_2, SnO_2 and CuO hollow spheres was similar with the above method except replacing the mixed metal salts as the corresponding single metal salt.

Characterization

The prepared samples were studied by the powder X-ray diffraction which were performed on a Bede D1 system operated at 20 kV and 30 mA with Cu Kα radiation (λ = 1.5406 Å). The Scanning electron microscopy (SEM; S-4800, Hitachi) and transmission electron microscopy (HR-TEM, FEI F20) were used to identify the morphology and crystal structure of the hollow spheres. The XPS spectra were recorded on a Thermo ESCALAB-250 spectrometer using a monochromatic Al Kα radiation source (1486.6 eV). The binding energies determined by XPS were corrected by reference to the adventitious carbon peak (284.6 eV) for each sample. Room-temperature photoluminescence (PL) measurement was carried out with excitation by a 325 nm line of a He–Cd laser to evaluate the emission properties of the hollow spheres. The optical properties were tested on a Shimadzu UV3600 ultraviolet-visible spectrophotometer.

Photocatalytic Test

The photoreactor was designed as a glass vessel under light source and the suspension included the hollow spheres catalyst (20 mg), and an aqueous RB (100 mL, 20 mg/L) completely under the light source. The suspension was stirred in the dark for 5 hours to obtain a good adsorption-desorption equilibrium between the organic molecules and the catalyst surfaces. The temperature of the suspension was maintained at room temperature by circulating water, and the system was open to the air. The suspension was exposed to the irradiation of a 300 W Xe lamp at room temperature. The full range light had the photo-energy of 235 mW/cm^2 and the visible light was obtained by fitted with a cutoff filter (λ > 420 nm) with 138 mW/cm^2 photo-energy. Then the measurement of RhB degradation was carried out on a UV-Vis spectroscopy (Shimadzu UV3600).

Results and discussion

The strategy used to obtain the hybrid nanostructures could be divided into three steps **(Figure 1)**: (1) the adsorption of different metal ions into the surface of carbon spheres; (2) calcination of the adsorbed composite spheres in air to remove the carbon core, which resulted in mixed metal oxide hollow spheres; and (3) the subsequent annealing process to form hybrid nanostructures. There was an essential difference between this approach and traditional wet chemical strategies. In traditional synthesis processes, an unequal precipitation process of the different metal ions was inevitable and the experimental conditions must be precisely controlled to avoid the agglomeration phenomenon.[16,21]

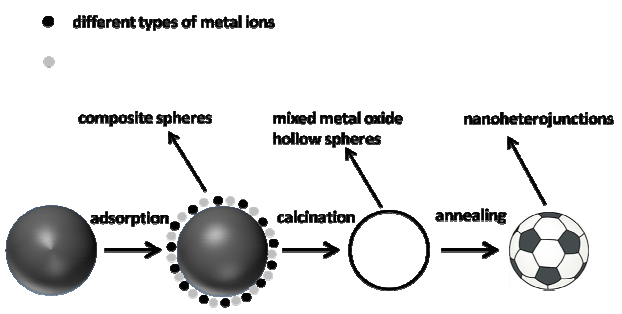

Figure 1. Schematic illustration of the preparation of new type of hybrid nanostructures.

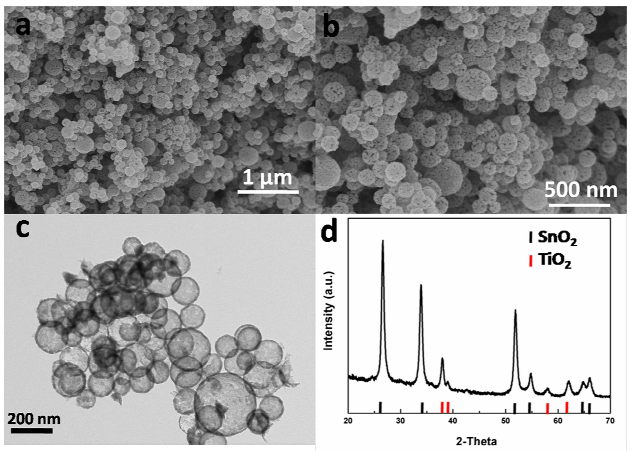

Figure 2. (a) and (b) are the SEM and enlarged SEM images of the TiO_2/SnO_2 hybrid nanostructures, respectively and (c) is the corresponding TEM image. (d) is the XRD pattern of the annealed TiO_2/SnO_2 hybrid nanostructures.

However, in our method, the templates had large numbers of -OH and -C=O groups on their surface[28] and the multiple metal ions were absorbed into the surface of the carbon spheres. Consequently, the uneven precipitation was naturally avoided.

The typical SEM images of the TiO_2/SnO_2 hollow spheres after annealing were shown in **Figure 2**. It could be seen that the perfect hollow spheres were formed and the average diameter of the hollow spheres was about 150 nm (Figure 2a). The enlarged SEM images (Figure 2b) indicated that the shell of the spheres was composed of nanoparticles with small size. In addition, there were many pores in the shell, which should be caused by the oxidation gas when the carbon cores were removed. And the low-magnification TEM image of the TiO_2/SnO_2 hollow spheres shown in Figure 2c clearly demonstrated the hollow characteristic of these structures. The XRD results of the TiO_2/SnO_2 hollow spheres after annealing at 450 °C were shown in Figure 2d. In this curve, some diffraction peaks could be perfectly indexed to the TiO_2 phase (PDF#65-1119). Whereas, apart from the TiO_2 peaks, there were the cassiterite SnO_2 peaks (PDF#41-1445) appeared in Figure 2d. Hence, it could be deduced that the TiO_2 phase was coexisted with the SnO_2 phase in the TiO_2/SnO_2 hollow spheres rather than the bimetallic compounds. In addition, the XRD peaks of TiO_2 and SnO_2 for the hollow spheres did not shift clearly compared with the corresponding pure phases. This indicated that there was no heavily doped solid solution formed in this system.

In the synthesis processes, the annealing process played a pivotal role in the formation of nanoheterojunctions. As a typical example, we investigated the phases and crystalline transformation of TiO_2/SnO_2 hollow spheres during the different processes. Apart from the diffraction peaks of SnO_2, we found no diffraction peaks indexed to the TiO_2 phase in the XRD pattern of the hollow spheres when it just finished the calcination process (**Figure 3a**). Furthermore, the HRTEM image revealed that a disordered outer layer was surrounded by the nanocrystalline cores in the shell of the hollow spheres (Figure 3b). The results indicated that the TiO_2 were not highly crystallized when it was only experienced the calcination process. After the annealing process, the XRD curve in Figure 3c indicated that some diffraction peaks indexed to the TiO_2 appeared in the annealed hollow spheres and the HRTEM image of the shells revealed the

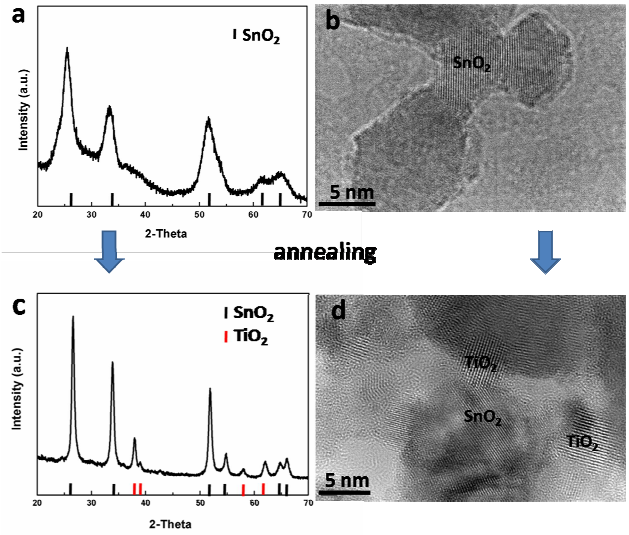

Figure 3. (a), (c) are the XRD patterns and (b), (d) are the HRTEM images of the TiO_2/SnO_2 hybrid nanostructures experienced the calcination and annealing processes respectively.

presence of SnO_2 and TiO_2 crystalline lattices (Figure 3d). Therefore, a subsequent annealing process was essential to maintain the highly crystallized nanoparticles of the two metal oxides.

In order to study the morphology and crystal structure of the TiO_2/SnO_2 hybrid nanostructures deeply, the transmission electron microscopy (TEM) observations were shown in **Figure 4**. The TEM image of the TiO_2/SnO_2 hollow spheres shown in Figure 4a clearly demonstrated the thickness of the shell was about 7 nm and large numbers of pores were existed in the shell. Meanwhile, Figure 4b displayed the high-resolution images of the shells of the TiO_2/SnO_2 hollow spheres. It could be seen clearly that the shell was composed of nanoparticles in a football-like structure and each nanoparticles were attached to several other nanoparticles, which revealed the simultaneous presence of the different types of nanoparticles. The size of particles comprised the shell were variable and most of them were in the range from 3 to 10 nm (Figure 4b). The HRTEM images of TiO_2/SnO_2

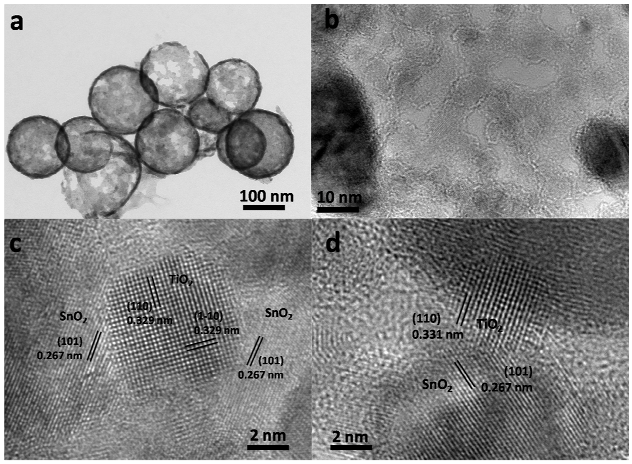

Figure 4. (a) is the enlarged TEM image of the TiO_2/SnO_2 hybrid nanostructures. (b) is the HRTEM image of the shell of TiO_2/SnO_2 hybrid nanostructures. (c) and (d) are the HRTEM images of the TiO_2/SnO_2 nanoheterojunctions in different positions of the TiO_2/SnO_2 hybrid nanostructures.

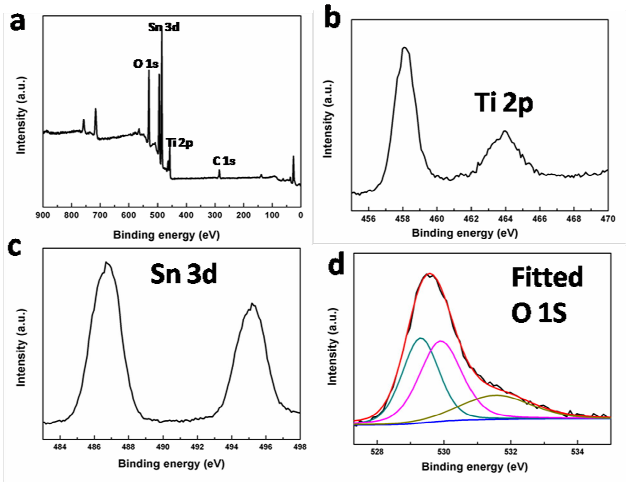

Figure 5. (a) is the XPS spectra of the TiO_2/SnO_2 hybrid nanostructures (b), (c) are the XPS spectra for Ti2p, Sn3d and (d) is the fitting XPS spectra for the O1s.

disclosed that all the species had clear lattice fringes, suggesting that both TiO_2 and SnO_2 had crystalline nanostructures after annealing process. Moreover, compared with the previous TiO_2/SnO_2 hybrid nanostructures,[13-15] we found the TiO_2 and SnO_2 nanoparticles had excellent crystalline compatibility at the interface. The vertical d-spacings of the lattice fringes were measured to be 0.329 nm, corresponding to the (110) and (1-10) planes of tetragonal TiO_2 (Figure 4c). These values of the adjacent nanoparticles were close to the (101) planes of SnO_2 with interplanar spacings of 0.267 nm (Figure 4c). And we attributed it to the recrystallization of the TiO_2 nanoparticles which were crystallized on the SnO_2 nanoparticles during the annealing process. Moreover, compared with the previous TiO_2/SnO_2 hybrid nanostructures,[13-15] we found the TiO_2 and SnO_2 nanoparticles had excellent crystalline compatibility at the interface. And we attributed it to the recrystallization process of the TiO_2 nanoparticles which were crystallized on the SnO_2 nanoparticles during the annealing process. The distinguished interfaces between the TiO_2 and SnO_2 nanoparticles could be observed in Figure 4c, d, suggesting that the hybrid nanostructures have been formed between the TiO_2 and SnO_2 nanoparticles in the shell of the mixed metal oxides hollow spheres. The HRTEM observations showed the shell had clearly crystalline lattices. And in conjunction with the thickness of the shell was only 7 nm, we could confirmed that the nanoparticles in the shell were distributed in a single-layer. Therefore, it leaded to the monolayer distribution of the hybrid nanostructures rather than the serious stacking in previous reports.[13-15]

We examined the compositions and chemical states of TiO_2/SnO_2 hybrid nanostructures with x-ray photoelectron spectroscopy (XPS). The fully scanned spectra (**Figure 5a**) demonstrate that Ti, Sn, and O elements existed in TiO_2/SnO_2 hollow spheres. As shown in **Figure 5b**, there were two peaks in the Ti 2p region respectively and the peak located at 458.1 eV corresponded to the Ti 2p 1/2 and another one located at 463.8 eV was assigned to Ti 2p 3/2 . The peaks for Ti 2p in the hybrid nanostructures showed no shift compared with the standard bare TiO_2 (Figure S1a), confirming that the structure of TiO_2 remained intact after synthesis of hybrid nanostructures. In Figure 5c, the Sn 3d 5/2 peak was located at 486.7 eV and the Sn 3d 3/2 peak was found

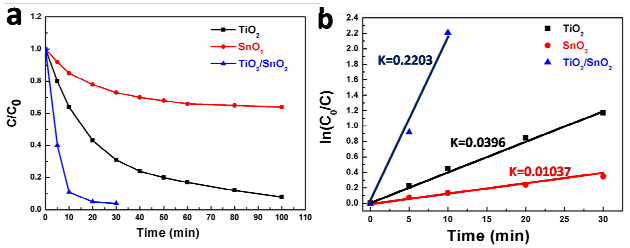

Figure 6. (a) The concentration changes of RhB dye as a function of irradiation time under full range light with TiO_2, SnO_2 and the TiO_2/SnO_2 nanoheterojunctions, respectively. (b) Kinetic linear simulation curves of RhB photocatalytic degradation with the different samples shown in Figure 6a.

at 495.1 eV, indicating that the valence state of Sn was +4 (Figure S1b). Furthermore, the wide and asymmetric peak of O 1s spectrum in the hybrid nanostructures demonstrated that there could be more than one chemical state according to the binding energy. Fitting the O 1s XPS, the O 1s XPS spectrum was fitted to three kinds of chemical states. Based on the previous reports, it should be included the crystal lattice oxygens O-Ti-O (529.3 eV), O-Sn-O (529.9 eV) and the interface oxygens with increasing binding energy (531.6 eV) (Figure 5d). The Brunauer – Emmett – Teller (BET) gas sorptometry measurements have been conducted to examine the TiO_2/SnO_2 hybrid nanostructures (Figure S2). It showed the specific surface area of the TiO_2/SnO_2 hybrid nanostructures was 328 $m^2 g^{-1}$. Therefore, the high surface area was able to provide enough catalytic surface sites of the reactants to increase the rate and efficiency of the reactions.

The photocatalytic activities of the pure SnO_2, TiO_2 hollow spheres and the TiO_2/SnO_2 hybrid nanostructures under full range light were evaluated by the photocatalytic oxidation of the RhB dye (**Figure 6**). The degradation of RhB dye for the pure TiO_2[29] and SnO_2[30] hollow spheres was presented as a reference in this test. As expected from the initial design, the degradation time for TiO_2/SnO_2 hollow spheres was only 1/8 for the pure TiO_2 hollow spheres. It exhibited an ultrahigh photocatalytic activity which had never seen before in the presented hybrid nanostructures.[17-26] For a better comparison of the photocatalytic efficiency of the above samples, the kinetic analysis of degradation of RhB was discussed. The kinetic linear simulation curves of the photocatalytic degradation of RhB over the above samples showed that the degradation reactions followed an apparent first order kinetics model:

$$\ln C_0/C = kt$$

where k is the apparent first order rate constant (min^{-1}). The determined k for different catalysts was summarized in Figure 6 b. It was indicated that the photocatalytic reactivity order was TiO_2/SnO_2 hybrid nanostructures >> TiO_2 hollow spheres > SnO_2 hollow spheres, which was consistent with the activity studies in Figure 6a. Therefore, after the comparison among those materials, this new type of TiO_2/SnO_2 hybrid nanostructures exhibited an ultrahigh photocatalytic activity.

The PL spectra were related to the transfer behavior of the photo-generated electrons and holes so that it could help to explain the above photocatalytic performance of the new type of the hybrid nanostructures. **Figure 7** showed the PL spectra of pure SnO_2, TiO_2 hollow spheres and the TiO_2/SnO_2 hybrid nanostructures. It could be seen that both the pure TiO_2 and SnO_2 hollow spheres

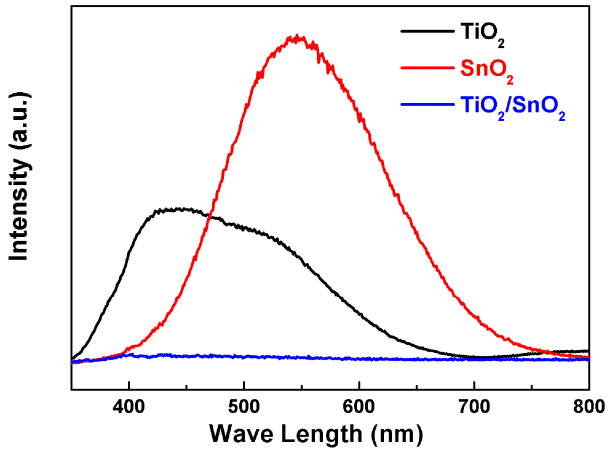

Figure 7. The PL spectra of the TiO_2, SnO_2 hollow spheres and the TiO_2/SnO_2 nanoheterojunctions, respectively.

exhibited obvious PL emission signals upon irradiation with 325 nm light. What's more, compared with the above two hollow spheres, the TiO_2/SnO_2 hybrid nanostructures depicted nearly no emission signal in this test. And it exhibited a quenching phenomenon both in the UV and visible light regions. Therefore, the direct recombination of the photo-generated carriers was vanished in the presence of TiO_2/SnO_2 hybrid nanostructures. For both of the TiO_2 and SnO_2 were the direct gap semiconductors, the PL emission characteristics of the TiO_2/SnO_2 hybrid nanostructures could confirmed its highly efficient separation of the photo-generated carriers.

To clear the separation mechanism, a proposed energy band structure diagram of the SnO_2/TiO_2 hybrid nanostructure was elucidated schematically in Figure 8. When the SnO_2 and TiO_2 formed the heterojunction, the electron transfer occurred from TiO_2 to SnO_2 while the hole transfer occurred from SnO_2 to TiO_2 until the system attained equilibration. Meanwhile, an inner electric field was built in the interface between TiO_2 and SnO_2 because of the electron and hole transfers. Thus, compared with the conventional TiO_2/SnO_2 composites, we could conclude the advantages of this new type of TiO_2/SnO_2 hybrid nanostructures. The small size of the hybrid nanostructures could effectively

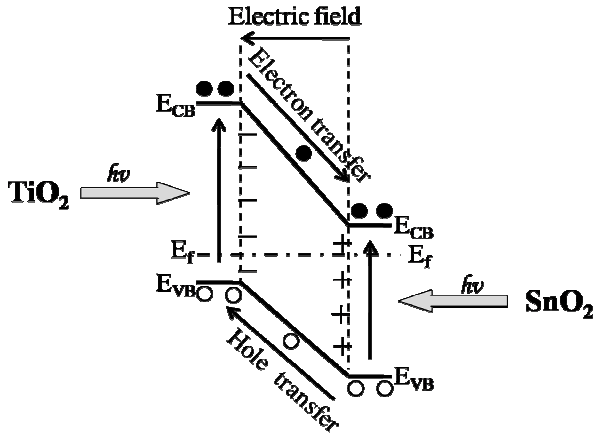

Figure 8. Schematic Diagram Showing the Energy Band Structure and Electron-Hole Pair Separation in the TiO_2/SnO_2 nanoheterojunction.

the diffusion distance for carriers. What's more, the excellent crystalline compatibility and single-layer distributed arrangement of nanoheterojunctions could highly separate the photo-generated carriers. Therefore, this new type of hybrid nanostructures could has an ultrahigh separation efficiency to the photo-induced carriers which never seen before. Furthermore, the ultrahigh surface area of the hybrid nanostructures was able to provide enough catalytic surface sites; thus, this new type of the hybrid nanostructures was resulted in an ultrahigh photocatalysis activity for environmental applications. And this synthesis strategy has been extended to other hybrid nanostructures successfully, such as, the TiO_2/CuO and TiO_2/Cr_2O_3 hybrid nanostructures (see supporting information). These results indicated that it was a general route for the synthesis of the new type of hybrid nanostructures.

Conclusion

In summary, a new type of hybrid nanostructures was obtained by ions adsorption and templating approaches and we fabricated the TiO_2/SnO_2 hybrid nanostructure as a typical example. The presented hybrid nanostructures have small grain size in the range from 3 to 10 nm and large surface area higher than 300 m^2 g^{-1}. What' more, because of the ultrathin shell and annealing process, the hybrid nanostructures had high crystalline compatibility at the contact interface and monolayer distributed structure. The PL analysis indicated that this new structure could completely separate the photo-generated holes and electrons. And owing to the enhanced separation efficiency of the photo-generated carriers, the TiO_2/SnO_2 hybrid nanostructures have ultrahigh photocatalytic activity than the TiO_2 and SnO_2 hollow spheres for the degradation of the RhB dye. We attributed it to the enhanced separation efficiency of the photo-generated carriers in the presence of the hybrid nanostructures. Furthermore, this strategy could extend to other materials system to synthesize the corresponding hybrid nanostructures.

Notes and references

a State Key Laboratory of Silicon Materials
Department of Materials Science and Engineering
Zhejiang University
Hangzhou 310027 (P.R. China)
b Cyrus Tang Center for Sensor Materials and Applications
Zhejiang University
Hangzhou 310027 (P.R. China)
Correspondence and requests for materials should be addressed to L.P. Zhu (Email: zlp1@zju.edu.cn, Fax: (+86) 571-87951958)

† Electronic Supplementary Information (ESI) available

‡ This work was supported by National Natural Science Foundation of China 51372224, Program for Innovative Research Team in University of Ministry of Education of China（IRT13037）, and National Science and Technology Support Program (2012BAC08B08)

1. H. Tong, S. Ouyang, Y. Bi, N. Umezawa, M. Oshikiri and J. Ye, *Adv. Mater.,* 2012, **24**, 229.
2. X. Chen, S. Shen, L. Guo and S. S. Mao, *Chem. Rev.,* 2010, **110**, 6503.
3. Z. Zou, J. Ye, K. Sayama and H. Arakawa, *Nature*, 2001, **414**, 625.
4. A. Sitt, I. Hadar and U. Banin, *Nano. Today.*, 2013, **8**, 494.
5. D. Wang, T. Kako and J. Ye, *J. Am. Chem. Soc.*, 2008, **130**, 2724.
6. A. Mills and S. Le Hunte, *J. Photo.chem. Photobio. A: Chem.*, 1997, **108**, 1.
7. K. Tennakone and J. Bandara, *Appl. Catal. A.*, 2001, **208**, 335.
8. J. Nowotny, *Energy. Environ. Sci.,* 2008, **1**, 565.
9. A. Kudo and Y. Miseki, *Chem. Soc. Rev.*, 2009, **38**, 253.
10. L. Zheng, Y. Zheng, C. Chen, Y. Zhan, X. Lin, Q. Zheng, K. Wei and J. Zhu, *Inorg. Chem.*, 2009, **48**, 1819.
11. K. Maeda, K. Teramura, D. Lu, T. Takata, N. Saito, Y. Inoue and K. Domen, *Nature*, 2006, **440**, 295.
12. Y. Wang, S. Li, H. Shi and K. Yu, *Nanoscale*, 2012, **4**, 7817.
13. J. Qian, P. Liu, Y. Xiao, Y. Jiang, Y. Cao, X. Ai and H. Yang, *Adv. Mater.*, 2009, **21**, 3663.
14. Y. Cao, X. Zhang, W. Yang, H. Du, Y. Bai, T. Li and J. Yao, *Chem. Mater.*, 2000, **12**, 3445.
15. C. Wang, C. Shao, X. Zhang and Y. Liu, *Inorg. Chem.*, 2009, **48**, 7261.
16. X. Xu, G. Yang, J. Liang, S. Ding, C. Tang, H. Yang, W. Yan, G. Yang and D. Yu, *J. Mater. Chem. A.*, 2014, **2**, 116.
17. S. Ponja, S. Sathasivam, N. Chadwick, A. Kafizas, S. M. Bawaked, A. Y. Obaid, S. Al-Thabaiti, S. N. Basahel, I. P. Parkin and C. J. Carmalt, *J. Mater. Chem. A.*, 2013, **1**, 6271.
18. Q. Huang, F. Kang, H. Liu, Q. Li and X. Xiao, *J. Mater. Chem. A.*, 2013, **1**, 2418.
19. E. H. Sargent, *Nat. Photon.*, 2012, **6**, 133.
20. W. W. Wang, Y. J. Zhu and L. X. Yang, *Adv. Func. Mater.*, 2007, **17**, 59.
21. X. Lü, F. Huang, X. Mou, Y. Wang and F. Xu, *Adv. Mater.*, 2010, **22**, 3719.
22. S.-I. In, D. D. Vaughn and R. E. Schaak, *Angew. Chem. Int. Ed.*, 2012, **51**, 3915.
23. L. Zhi, Y.-S. Hu, B. E. Hamaoui, X. Wang, I. Lieberwirth, U. Kolb, J. Maier and K. Müllen, *Adv. Mater.*, 2008, **20**, 1727.
24. A. G. Pattantyus-Abraham, I. J. Kramer, A. R. Barkhouse, X. Wang, G. Konstantatos, R. Debnath, L. Levina, I. Raabe, M. K. Nazeeruddin, M. Grätzel and E. H. Sargent, *ACS. Nano.*, 2010, **4**, 3374.
25. S. Mridha and D. Basak, *J. Appl. Phys.*, 2007, 101.
26. K. Kamata, K. Maeda, D. Lu, Y. Kako and K. Domen, *Chem. Phys. Lett.*, 2009, **470**, 90.
27. X. Sun and Y. Li, *Angew. Chem. Int. Ed.*, 2004, **43**, 597.
28. X. Sun and Y. Li, *Angew. Chem. Int. Ed.*, 2004, **43**, 3827.
29. X. Sun, J. Liu and Y. Li, *Chem. Eur. J.*, 2006, **12**, 2039.
30. J. Zhang, J. Liu, Q. Peng, X. Wang and Y. Li, *Chem. Mater.*, 2006, **18**, 867.

Yaguang Li and Liping Zhu*

A new type of hybrid nanostructures: complete photo-generated carriers separation and ultrahigh photocatalytic activity

A new type of hybrid nanostructures could completely separate the photo-generated carriers and exhibited ultrahigh photocatalytic activities.